Ruthenium- and cobalt-based artificial metalloenzymes for photocatalytic water oxidation in artificial photosynthesis

Polanco Rivas, E.A.

Chapter
2

Screening of Co– and Ru–complexes with Haem proteins for protein–complex interaction

Part of this chapter has been published as a research article: _A screening method for binding synthetic metallo–complexes to haem proteins. Opdam, L.V.; Polanco E.A.; de Regt, B.; Lambertina, N.; Bakker, C.; Bonnet, S.; Pandit, A. Analytical Biochemistry. **2022**, 653, 114788._[1]

2.1. Introduction

Developing artificial metalloenzymes (ArM) requires practical strategies. On the one hand produce significant amounts of a conjugate of a protein and a metal complex. On the other hand, to find the best possible protein–metal complex association, *i.e.*, the couple of building blocks that when bound to each other, may perform a desired function. The actual location of the metal complex in the conjugate will depend both on the nature of the metal complex precursor, and on the coordination properties of the protein. The natural cofactor–binding pocket of a protein is a common target to redirect the function of an enzyme by conjugation with an alternative (artificial) cofactor.[2,3] In some cases, the chemical features of such alternative metal cofactor, such as its size, hydrophilicity, or planarity, resemble that of the natural cofactor of the protein. On the other hand, it may be tricky with ArMs to characterize the binding mode of an artificial cofactor to the protein scaffold. Typically, a multitude of characterization techniques are required for that purpose, such as mass spectrometry, UV–vis spectroscopy, circular dichroism (CD), electron paramagnetic resonance (EPR), and/or inductively coupled plasma mass spectrometry (ICP–MS). However, by far the most common techniques to analyse the interaction between proteins and small molecules is sodium dodecyl sulfate polyacrylamide gel electrophoresis, also called SDS–page. For such technique, a right choice of the gel type that is used for observing the formation of a protein–cofactor conjugate is essential. In the route towards the production of an ArM capable of performing photocatalytic water oxidation, we engaged into developing a protocol to screen the interaction between different small–molecule water oxidation catalysts based on ruthenium and cobalt, and two haem proteins (Figure 2.1).
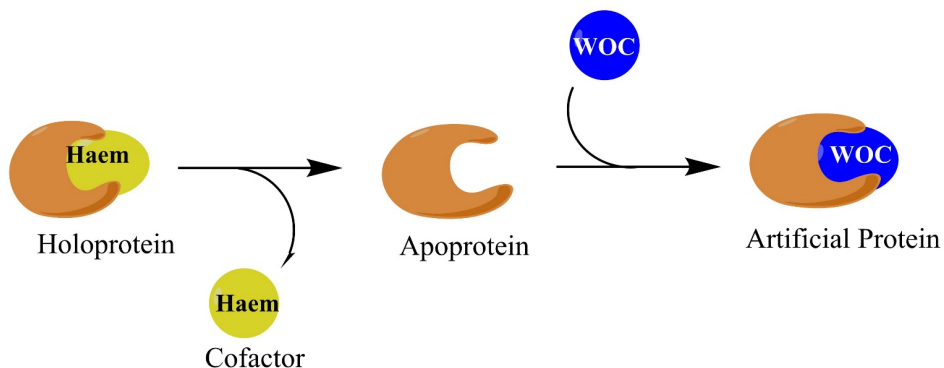
Figure 2.1. Representation of the strategy used on this chapter to prepare a water–oxidizing artificial protein.

Ruthenium is a d^6 second–row transition metal that has shown particularly good catalytic properties especially for water oxidation. In fact, as mentioned in Chapter 1, most reported water oxidation catalysts (WOC) showing high turnover number (TON) are based on ruthenium.[4,5] A majority of these compounds are introduced in the reaction medium in the oxidation state +II, they have a hexacoordinated environment and are based on nitrogen ligands (polypyridines). Plus, they bear a negatively charged coordinating group bound to the metal, which stabilizes the high oxidation states required for showing good catalytic properties. Cobalt is another attractive transition metal for water oxidation catalysis.[6] Being more earth–abundant it is often considered as being more sustainable than ruthenium. Many cobalt complexes have been reported to perform water oxidation in chemical, electrochemical, or photochemical conditions, though at a lower rate and with lower stability than many ruthenium WOCs.[7] For these reasons, in this chapter a library of Ru– and Co–complexes (Figure 2.2) was screened towards the production of an ArM that could catalyse photocatalytic oxygen evolution using water as source of electrons.
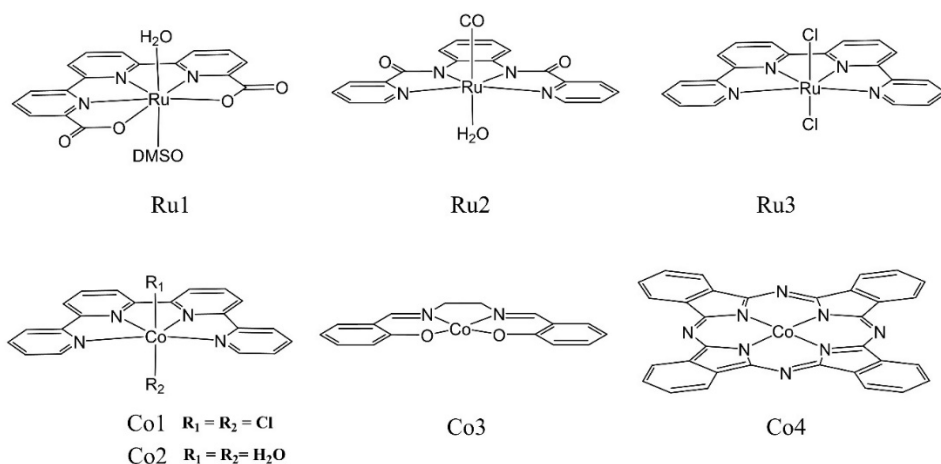
Figure 2.2. Ruthenium and cobalt complexes screened for the generation of a water–oxidizing artificial metalloenzyme.

On the protein side, a set of two haem proteins, Cytochrome B5 (**CB5**) and Myoglobin (**Myb**), were selected as ArM scaffold for the binding of the WOC metal complexes (Figure 2.3). The particularity of these proteins relies on their binding pocket. As showed in Chapter 1 (Figure 1.7 and Figure 1.8), they contain histidines residues that coordinate the natural cofactor of the protein in the catalytic pocket. These residues bind axially to haem, providing two coordination anchors for the metal center. Nitrogen–based ligands are well–known to offer good interaction with ruthenium and cobalt. Altogether, these attractive features make these two proteins interesting candidates for the accommodation of water oxidation catalysts such as **Ru1**–**Ru3** or **Co1**–**Co4** in the binding pocket. Herein, we developed a quick and efficient method using semi–native SDS–gels to study the interaction between the water oxidation complexes and the *apo* form of **CB5** and **Myb** to produce haem–like artificial metalloenzymes for photocatalytic water oxidation.

Cytochrome B5 **(CB5)**   Myoglobin (**Myb**)
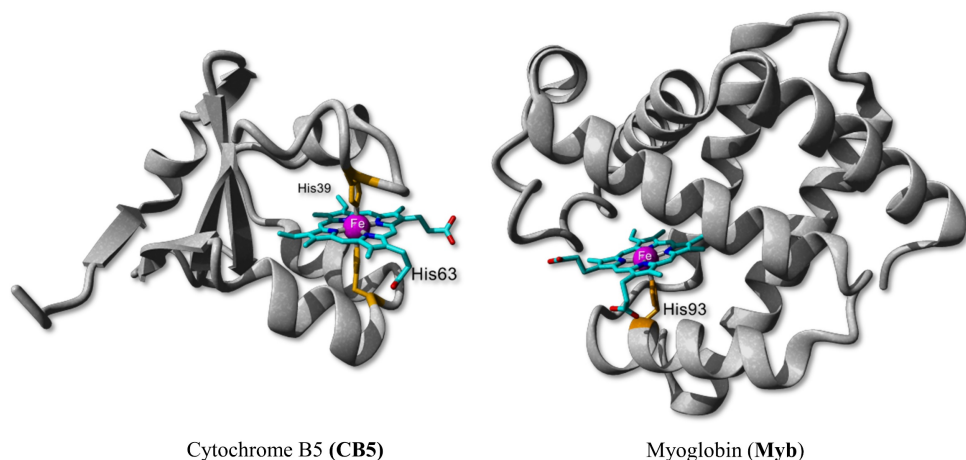
Figure 2.3. Haem proteins used to produce ArMs as WOC: Cytochrome B5 (**CB5**, left, PDB:1CYO) and Myoglobin (**Myb**, right, 5D5R). The proteins are shown with the natural haem cofactor in the binding pocket, and the metal–binding histidines residues coloured in orange.

2.2. Results

2.2.1. Electrophoresis gel selection

Electrophoresis it is a simple and yet useful technique to study proteins.[8] It can provide information about the purity, the presence or absence of interaction between a protein and a small molecule, or even the aggregation state of the protein.[9,10] However, the composition of the gel used to perform electrophoresis strongly influences the information you can obtain from a gel. **CB5** was chosen as model protein to start the screening of the conditions to obtain optimal binding of the metal complex to the proteins. First, the *apo* form of the protein was prepared. Then, the *apo* protein was incubated in presence of the different metal complexes in given conditions, and finally all mixtures were studied and compared by gel electrophoresis (Figure 2.4). For this, a stock solution of each catalyst was prepared in water or DMSO, then mixed with a 10 µM solution of *apo***CB5** in different protein:complex ratios: 10:10, 10:50 and 10:100 µM, in a 20 mM phosphate buffer pH 7.2, keeping the sample in dark at 4 °C during 3 days (See Experimental section). Each protein–metal complex mixture was run in three different types of gel:

denaturing, native, and semi–native. Denaturing gels, where the gel contains a given percentage of Tricine and SDS, are commonly used for separate proteins that are smaller than 30 kDa.[11] However, these kind of gels shows proteins which have a covalent bond with a substrate or cofactor. In native gels, no denaturing agent is used in the gel, running buffer, or cracking buffer (SDS and β–mercaptoethanol). These gels usually show a new bands whenever a strong interaction is taking place, such as a covalent bond between a small molecule and the protein.[12] For semi–native gels both the gel itself and the running buffer contains SDS, but the cracking buffer is prepared in absence of denaturing agents, SDS, and β–mercaptoethanol. As shown below, these different types of gel have different capacity to visualize the interaction between *apo*CB5 and the 7 complexes in our library. Native gels did not show good resolution between the free *apo* protein and the adduct with cobalt complexes: no new band was clearly visible in our reaction conditions, but smeared bands (Figure 2.4C). In the case of denaturing gels, the resolution of the gels did not give any information about the formation of new complex–protein adduct, which might be related to the small weight difference between the free protein and the adduct protein–complex is below the threshold for this gel. (Figure 2.4B). Among the three tested gels, the semi–native one showed the best resolution (Figure 2.4A) and indicated in many cases the formation of a new band different from that of the *apo* protein. The observation of clear new bands indicated the formation of well–defined adducts between the protein and complexes **Co2** and **Co3**. For these reasons, the semi–native gel was chosen to proceed further with the optimization of the reaction conditions for the formation of the new artificial metalloenzymes.
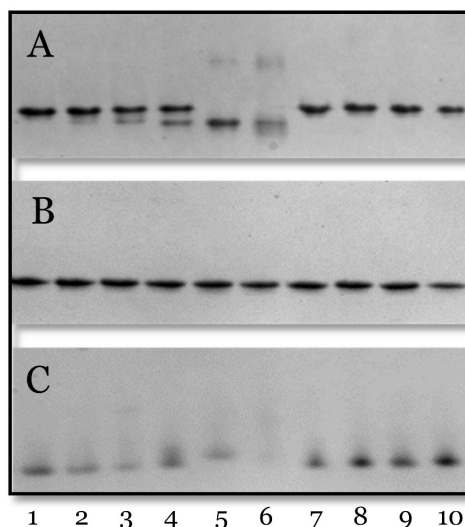
Figure 2.4. ArM formation between *apo*CB5 and cobalt complexes **Co2**, **Co3**, or **Co4**, screened using semi–native (**A**), denaturing (**B**), or native (**C**) gel electrophoresis. Lane 1 to 3, **Co2**; Lane 4 to 6, **Co3**; lane 7 to 9, **Co4**; Lane 10 is *apo*CB5. Concentration of the cobalt complex is 10, 50 or 100 μM from left to right for each complex set. Conditions: 20 mM phosphate buffer, pH 7.2, temperature 4 °C, in the dark, reaction time = 3 days, [*apo*CB5]=10 μM.

2.2.2. Optimizing the protein:complex ratio for ArM production

In general, the protein:complex ratio needed to be optimized for the formation of ArM. Here, three protein:complex ratios were used, 1:1, 1:5 and 1:10. ArM preparation was performed in a sodium phosphate pH 7.2 buffer in the dark at 4 °C. In such conditions, the proteins were stable notably towards denaturation. We also prevented, at that stage, any light irradiation to avoid that unknown photochemical reaction may influence the final hybrid. The insoluble metal complexes were first dissolved in DMSO before addition to the protein–containing buffer (10 µM), keeping the percentage of DMSO lower than 10% in the reaction mixture. As seen in Figure 2.4, after 3 days reaction for ruthenium two of the complexes, **Ru2** and **Ru3**, showed a new band according to semi–native gel electrophoresis. Lanes 4–6 also demonstrated that an increase of the ruthenium complex concentration also

increased the intensity of the new band, which run below that of the *apo* protein. These results are an indication that the interaction of the complex with the protein is concentration dependent. Within three ruthenium compounds tested here, **Ru1** was the only complex that showed no interaction with **apoCB5** (Lane 1–3).
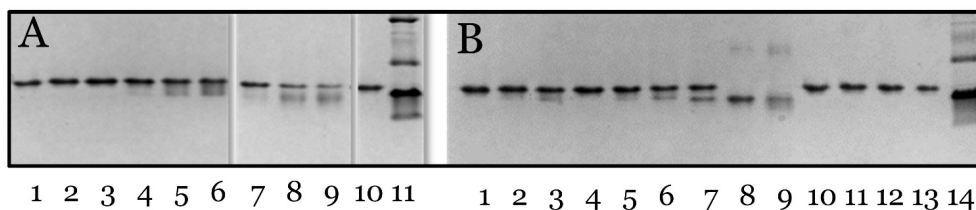
Figure 2.5. Semi–native SDS–gel electrophoresis analysis of the reaction between **apoCB5** and **Ru1**–**Ru3** or **Co1**–**Co4** complexes at increasing metal complex concentrations. (**A**) Ruthenium complexes: Lane 1 to 3, **Ru1**; Lane 4 to 6, **Ru2**; Lane 7 to 9, **Ru3**; Lane 10, **apoCB5**; Lane 11, protein reference ladder. (**B**) Cobalt complexes: Lane 1 to 3, **Co1**; Lane 4 to 6, **Co2**; Lane 7 to 9, **Co3**; Lane 10 to 12, **Co4;** Lane 13, **apoCB5**; Lane 14, protein reference ladder. Conditions: [Catalyst] = 10, 50 or 100 µM (from left to right for each complex), 200 µL samples were prepared in a 96–well plate, 20 mM phosphate buffer, pH 7.2, temperature 4 ºC, in the dark, 3 days, [**apoCB5**]=10 µM.

For the cobalt complexes, three out of the four tested complexes showed interaction with the protein (Figure 2.5B). **Co1** and **Co2** showed a similar pattern on the gel: a new, lower band appeared in presence of a medium concentration of the complex (50 µM, Lane 2 and 5, respectively). Like for **Ru2** and **Ru3**, when the concentration of the cobalt complex was increased to 100 µM, the intensity of the band related to the new complex–protein adduct increased (Lane 3 for **Co1** and Lane 6 for **Co2**), and when the concentration was diminished no new band could be observed anymore. The interaction was hence concentration–dependent here as well. For **Co4**, no new band formation could be observed at any of the concentrations tested. Clearly for **Co3** the interaction with **apoCB5** was stronger than with all other metal complexes in this library. At a **Co3** concentration of 10 µM a new band was already visible, while for all other complexes only **apoCB5** could be seen at such

low concentration. In addition, when the concentration of the catalyst was increased to 50 µM, the band of **apoCB5** became invisible, and only the new band characteristic for the new protein–complex adduct could be observed. Altogether these facts suggest that the affinity between **Co3** and the protein scaffold is strong in the tested conditions.

2.2.3. pH effect

In principle the pH of the reaction can also play a role during ArM preparation. Depending on the pK_a of all aminoacid residues that can be protonated, each protein is characterized by an isoelectric point (pI), which defines the pH at which the protein has a neutral charge.[13] As the pI value depends on the protein sequence, the charge of a protein may influence its interaction with a metal cofactor, in particular if this cofactor has a net charge. To see the effect of this parameter in our system, the binding of **apoCB5** with our library of metal complexes was tested in phosphate buffers at different pH: 6.0, 7.0 and 8.0. Given the results in our initial screening, two protein:complex ratios were selected for this experiment: 1:10 and 1:20. Also, 5 out of 7 complexes were selected for the pH screening based on previous protein–complex interaction results: **Ru2**, **Ru3**, **Co1**, **Co2** and **Co3**. For the ruthenium complexes **Ru2** and **Ru3** no significant difference in reactivity was observed at different pH's (Figure 2.6). The lower band, assigned to the new protein–complex species, was formed in similar amounts. As can be observed in the gel, for **Ru3** lanes 1, 3, and 5, showed a more intense band for the *apo* protein than for the new adduct. When the concentration of the complex was higher the band of the new adduct was more visible than that of the *apo* protein (Lanes 2,4 and 6). This effect correlated well to what was observed in previous section. A similar behaviour was observed for the cobalt complexes. For **Co3**, the band of the free *apo* protein disappeared in all lanes while the new band from the protein–complex adduct was clearly visible. For this adduct, a faint, higher band was observed that may be related to small amounts of a dimeric form of the protein, or a protein to which multiple molecules of **Co3**

have bound. Overall, according to these results pH did not significantly affect the interaction between *apo*CB5 and any of these metal complexes.
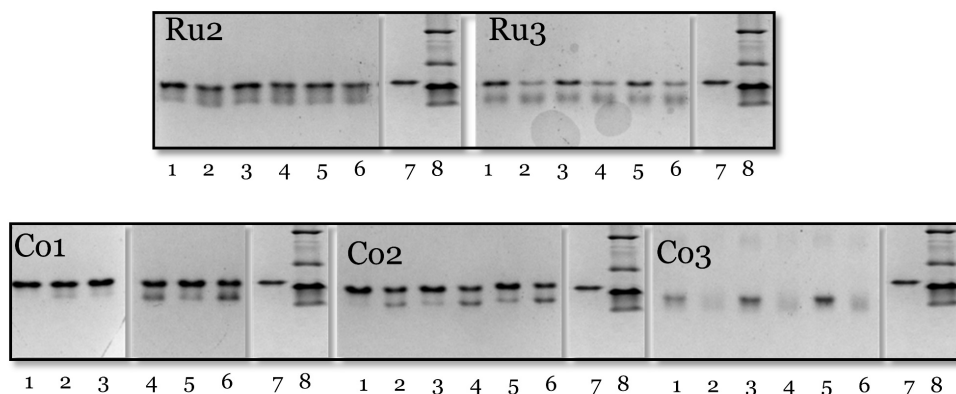
Figure 2.6. Effect of pH on the binding of ruthenium (top) and cobalt (bottom) complexes to *apo*CB5 according to semi–native SDS–gel. For each gel: complex concentration 100 µM (Lane 1,3 and 5) and 200 µM (Lane 2,4 and 6); Lane 1 and 2, pH 6; Lane 3 and 4, pH 7; Lane 5 and 6, pH 8; Lane 7, *apo*CB5; Lane 8, ladder. Conditions: 200 µL samples were prepared in a 96–well plate, 20 mM phosphate buffer, temperature 4 ℃, in the dark, 3 days, [*apo*CB5]=10 µM.

2.2.4. Effect of temperature and time on protein stability during ArM preparation.

It is known that proteins may have different behaviour at different temperatures. Some are very stable near the boiling point of water, while others alter their conformation or even denature at temperatures as low as room temperature.[14–16] On the other hand, the coordination of protein residues to the metal precursor is expected to become faster at higher temperatures. The effect of temperature and reaction time on the ArM formation was hence studied by incubating *apo*CB5 with **Ru2**, **Ru3**, **Co2** and **Co4** at 4, 20, and 40 ℃. The total incubation time was fixed at 72 h, and an SDS–page gel was measured every 24 h. To compare the effect of temperature in the reaction we first focused on the 24 h time point: a difference between the three temperatures was already visible at that moment (Figure 2.7). At 4 ℃, we observed

the same behaviour as in Figure 2.6: an extra band lower than the band of the *apo*CB5 protein became visible for all samples except for **Ru1**. At 20 ºC and 40 ºC, the band of the adduct for new ArM were more intense with **Ru2**, **Ru3** and **Co2** than at 4 ºC (Lanes 2,3 and 4). These results confirmed that heat increases the kinetics of the binding of the metal complexes to the *apo* protein, provided decomposition (or denaturation) remains low. For **Ru1** and **Co4** (Lanes 1 and 6), no change was visible when the temperature was raised, suggesting that those compounds did not bind at all to the protein at 24 h, even at temperature as high as 40 ºC.

Like high temperatures, the effect of longer reaction times might be beneficial for the binding of a protein to a metal complex, but it may also be harmful to the protein if the temperature is too high. After 48 h, the gel showed the same bands compared to the 24 h time point for all samples and all temperatures (Figure 2.7). At 72 h, however, only the samples that had been stored at 4 ºC remained intact. For the samples kept at 20 ºC, the sample containing **Ru1** could not be measured at 72 h due to solvent evaporation; for complexes **Ru2**, **Ru3** a smear on the gel was visible (Lanes 2,3). At 40 ºC, only the samples from **Ru1**, **Ru3**, **Co2** and **Co4** could be deposited on the SDS gel. These corresponded to samples still in solution, as for these complexes DMSO had been used to dissolve the catalyst before mixing with the protein. In these cases, **Ru1**, **Ru3** and **Co2** showed more smear than at 20 ºC. Overall, these results indicated that protein denaturation would occur when the protein was exposed at temperatures higher than 4 ºC for periods longer than 48 h.
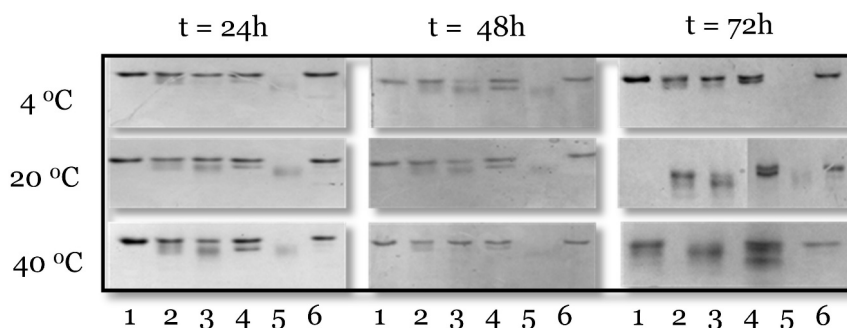
Figure 2.7. Temperature screening of the reaction between *apo*CB5 and Ru– and Co–complexes using SDS semi–native gel. Lane 1, **Ru1**; Lane 2, **Ru2**; Lane 3, **Ru3**; Lane 4, **Co2**; Lane 5, **Co3**; Lane 6, **Co4**. Conditions: 200 µL samples in a 96–well plate, 20 mM phosphate buffer, pH 7.2, in the dark, [*apo*CB5] = 20 µM, [catalyst] = 200 µM.

Observing that after 24 h incubation with *apo*CB5 some complexes showed total consumption of the *apo* protein, we hypothesized that the incubation time for some complexes might be shorter than for others. To address this, a set of complexes:*apo*CB5 mixtures were prepared with **Ru1**–**Ru3** and **Co1**–**Co3**, and the evolution of each sample was followed *vs*. time by SDS–gel by comparing t = 0 and t = 24 h (Figure 2.8). For **Co3**, at t = 0 h no *apo*CB5 could be seen anymore but only the complex–protein adduct (Lanes, 4,5 and 7, gel A, left), which was still visible in the gel after 24 h incubation (Lanes 5 to 7, gel A, right). For **Co2**, at t = 0 h a very faint second band was visible below the *apo*CB5 band (Lanes 1 to 3, gel A, left), which became more intense after 24 h reaction time. We interpret this band as the *apo*CB5–Co2 adduct (Lanes 2 to 4, gel A, right). For **Ru1**, no change was visible even after 24 h (Lanes 1 to 3, gel B). For **Ru2** at t = 0 h a faint band was visible that became more intense at 24 h reaction time (lanes 4 to 6, gel B, Figure 2.8). These results suggested that for the cobalt complexes in the library such as **Co3**, the incubation time required to prepare an ArM was shorter than for ruthenium complexes.

50
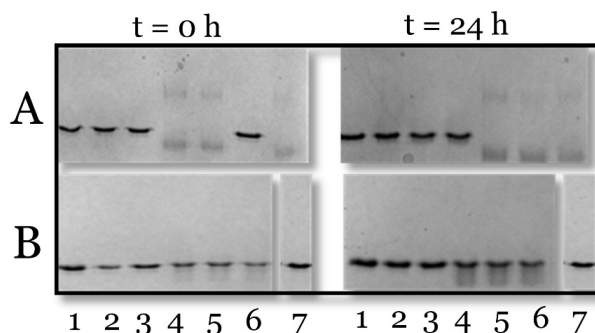
Figure 2.8. Influence of the reaction time on the reaction between *apo*CB5 and **Ru1**–**Ru2** or **Co2**–**Co3** according to SDS semi–native gel. (**A**) at t = 0 h, Lane 1 to 3, **Co2** (triplicate); Lane 4, 5 and 7, **Co3** (triplicate); Lane 6, *apo*CB5. At t = 24 h, Lane 1, *apo*CB5; Lane 2 to 4, **Co2** (triplicate); Lane 5 to 7, **Co3** (triplicate). (**B**) for both gels; Lane 1 to 3, **Ru1** (triplicate); Lane 4 to 6, **Ru2** (triplicate); Lane 7, *apo*CB5. Conditions: 200 µL samples were prepared in a 96–well plate by, 20 mM phosphate buffer, pH 7.2, temperature 4 ºC, in the dark, [*apo*CB5]=10 µM, [catalyst]=200 µM.

2.2.5. Mass spectroscopy

So far, the gel electrophoresis screening had provided information about the interaction of the water oxidation catalysts and the *apo*CB5 protein. According to this screening, **Ru2**, **Ru3**, **Co1**, **Co2** and **Co3** seem to be eligible for preparing ArM's. On the other hand, this technique provided no information on the nature of the adduct formed. ESI–MS was hence carried out as a second technique to characterize these adducts and better understand the gels. Here, *apo*CB5:complex 1:10 mixtures were incubated at a 10 µM protein concentration at 4 ºC in the dark overnight. Samples were passed through a Microspin p6 column (Bio-Rad) to remove the unbound metal complex before performing ESI mass spectrometry analysis (Table 2.1). All samples containing ruthenium showed the signal of *apo*CB5 (M = 10092 Da), suggesting the ruthenium complexes may be at least partially cleaved in the conditions of the mass spectrometer. For the mixture with **Ru2** the mass spectrum showed several additional peaks (Figure AI.3), the most abundant of which corresponded to *apo*CB5 + **Ru2** – H_2O (M = 10539 Da, calc = 10537 Da).

This result indicated that **Ru2** keeps the CO ligand once bound to the protein, and that only one axial ligand was substituted by a protein residue. Other peaks showed the formation of a protein–complex adduct; for example, M = 10981 Da (calc = 10983 Da) corresponded to one *apo*CB5 plus two molecules of **Ru2** each bearing one CO ligand. For **Ru3** even if gel electrophoresis had suggested the formation of a new species, no clearly identified signal was observed in the mass spectrum of the solution but the signal corresponding to *apo*CB5 (Figure AI.4). This result confirmed that the interaction between coordinating residues of the protein and the ruthenium center may not resist the conditions of the ESI mass spectrometer.

Table 2.1. Summary of the ESI mass spectrometry analysis of mixtures of *apo*CB5 (10 µM) and **Co1–Co3** or **Ru2–Ru3** (100 µM) incubated for 16 h at 4 °C.

Complex	Adduct	*apo*CB5 + complex (no axial ligands)[a]	*apo*CB5+ 2 complex (no axial ligands)[a]	*apo*CB5 + complex + 1 axial ligand[a]	*apo*CB5 + 2 (complex + 1 axial ligand)[a]
Ru2	Found	-	-	10539[b]	10981[b]
	Calculated	10511	10925	10537	10982
Ru3	Found	-	-	-	-
	Calculated	10503	10914	10538	10984
Co1	Found	10458	-	-	-
	Calculated	10461	10827	10493	10862
Co2	Found	10458	-	-	-
	Calculated	10491	10827	10479	10845
Co3	Found	10414	10742	-	-
	Calculated	10417	10742	-[c]	-[c]

*the signals showed in the table are Da. In all MS spectra the signal related to *apo*CB5 at 10092 Da was observed. [a]For the values not found in the ESI-MS spectrum symbol (-) was used. [b]The ligand bound to the complex is CO. [c]Co3 obtained commercially showed no axial ligands.

For all samples containing cobalt complexes a signal corresponding to an *apo*CB5–complex adduct was observed in the mass spectra (Table 2.1). For **Co1** and **Co2**, the mass spectra showed the signals for *apo*CB5 (M = 10092) and the *apo*CB5+**Co1/2** adduct (M = 10458 Da, calc = 10461 Da), where both axial ligands

had been cleaved (**Cl⁻** for **Co1** and **H₂O** for **Co2**). However, for **Co1** the signal intensity of the adduct ***apo*CB5–Co1** was lower than that of the adduct ***apo*CB5–Co2**: for the latter the ratio of the ***apo*CB5**:adduct was almost 1:1 (Figure AI.6), while for the former it was approximately 0.5:1 (Figure AI.5). This result supported the fact that these cobalt complexes have good protein–binding properties, as observed by SDS–page gel electrophoresis. **Co3** showed similar results as **Co1** and **Co2**, as the signal of the 1:1 ArM adduct was clearly visible (M = 10414 Da, calc = 10417 Da). An additional signal was observed (M = 10742 Da, calc = 10742 Da) corresponding to an adduct of ***apo*CB5** with two molecules of **Co3**. However, the relative intensity of the peak for ***apo*CB5** in this sample was lower than for the other complexes (Figure AI.7), which was in accordance with the lower intensity of the ***apo*CB5** band observed on SDS–page. According to this result, the binding between **Co3** and the protein was resisting the condition of mass spectrometry well, notably compared to what was observed with ruthenium complexes (Figure 2.8).

2.2.6. Myoglobin

Finally, to study what the influence of the protein structure was on the binding, we repeated the screening of the interaction between some of the metal complexes in our library (**Ru1**, **Ru2**, **Co1**, **Co3** and **Co4**) and another protein, *apo*–Myoglobin (***apo*Myb**), using the conditions optimized for ***apo*CB5** (Figure 2.9). For the sample with **Ru1,** no new band was observed in the gel (Lane 1, Figure 2.9). For **Ru2**, ***apo*Myb** showed the same result as with ***apo*CB5**: a smeared band in the SDS–gel was observed after 24 h, and no peak could be identified by mass spectrometry that would correspond to an adduct with the protein. For cobalt complexes, **Co1** and **Co4** showed a very faint new band on the gel. For **Co1**, the mass peaks showed the formation of two adducts: ***apo*Myb+Co1** (M = 17392 Da, calc = 17391 Da) and ***apo*Myb+Co1**+[**Co1**–2Cl⁻]+H₂O (M = 17776 Da, calc = 17778 Da) (Figure AI.10). The first adduct visible in the mass spectrum indicated that the chloride ligand was still bound to the Co center. But a second signal at 17776 Da suggested that another

molecule of **Co1** could bind to the protein scaffold, without any axial chloride ligands but with a molecule of water coordinated to cobalt. With **Co4** diferent signal in the cromatogram is observed, which showed a retention time diferent than *apo* – and *holo*Myb (Figure AI.12). For **Co3** the pattern on the SDS–page were similar to that observed with *apo*CB5, i.e., *apo*Myb band disappeared and was replaced by a new band related to a new *apo*Myb–**Co3** adduct. Mass spectrometry corroborated this hypothesis. The spectra of the *apo*Myb–**Co3** samples showed that up to 3 cobalt complexes could bind to the protein (Figure AI.11). These results showed that the best interaction between *apo*Myb and one of the complexes of the library corresponded to the complex that also interacted best with *apo*CB5.
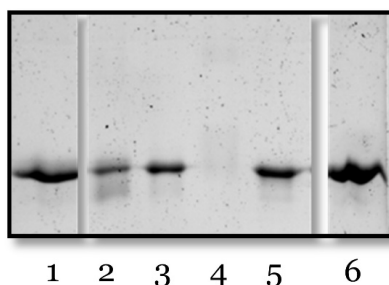
Figure 2.9. Semi–native SDS–gel of *apo*Myb and WOCs. Lanes: 1, **Ru1**; Lane 2, **Ru2**; Lane 3, **Co1**; Lane 4, **Co3**; Lane 5, **Co4**; Lane 6, *apo*Myb. Conditions: incubation 24 h at 4 °C, 20 mM phosphate buffer, pH 7, [*apo*Myb]=10 µM, [Catalyst]=100 µM.

2.3. Discussion

Semi–native SDS–page was found as the best gel electrophoresis technique for visualizing an interaction between a cobalt or ruthenium complex and either *apo*CB5 or *apo*Myb. This result was corroborated by ESI–MS, which also helped characterizing the adducts formed during the reaction. In addition, the affinity of nitrogen–based histidine ligands for cobalt(II) and ruthenium(II) metal centers was found strong enough to promote the binding of most complexes in this library. Two prominent factors were identified by SDS–gels in the optimization of the ArM

preparation: temperature and time. It is common knowledge that ruthenium complexes are thermally activated, i.e., that higher temperature may be needed to activate ligand exchange,[17] even if the free position in the coordination sphere is filled by a poorly–bound solvent molecule. However, we also observed here that longer exposition at temperatures higher than 4 ºC were not favourable for protein stability, which prevented proper attachment of the metal complex to the protein. Time wise, cobalt complexes were much faster to bind, and some cobalt complexes (such as **Co3**) even attached almost instantaneously to the protein scaffold. This difference is due to the position of cobalt and ruthenium in the periodic classification of the elements: cobalt is a first–row transition metal, and it is hence characterized by much faster ligand exchange compared to ruthenium, which is in the second row of the classification.

On the other hand, other factors than the nature of the metal center can play a role, too. In the ruthenium–based series of complex, the lack of interaction between **Ru1** and *apo*CB5 can probably be attributed to the too high hydrophilicity of the **Ru1** complex, which may decrease interaction with the hydrophobic binding pocket of the protein. For **Ru2**, which has a carbonyl (CO) and an aqua ligand in axial positions, the aqua ligand can be substituted by coordinating protein residues because of the *trans* effect generated by the CO ligand, which makes the aqua ligand more labile. On the other hand, the interaction between CO and the Ru center is very strong due to significant π–backbonding from the metal to the empty orbitals of CO; it is hence very difficult, under the reaction conditions tested here, to substitute CO by a protein residue such as a histidine. This result was confirmed by mass spectrometry, which showed that up to 3 molecules of **Ru2** may bind the *apo*CB5 scaffold, but always retaining CO bound. In addition, the binding of multiple units of **Ru2** suggests binding of the complex to the haem–binding site of the protein may not be that selective. In the case of **Ru3**, in aqueous solution the chloride (Cl$^-$) ligands can in principle dissociate to form a bis–aqua ruthenium specie,

$[Ru(qpy)(H_2O)_2]^{2+}$.[18,19] This specie bearing more labile ligands may bind faster to histidine residues, either in the binding pocket of the protein, or in other positions of the protein backbone. However, the mass spectrum and SDS–gel of the **apoCB5–Ru3** mixture showed that somehow this complex interacts in a different manner with the protein, giving a protein–complex system that cannot be identified. This observation suggests that a side–reaction between the complex itself and the protein might take place during incubation.

For the series of cobalt complexes, structurally speaking **Co1** and **Co2** are similar as their only differences are the nature of the axial ligand (Cl⁻ for Co1 and H_2O for **Co2**). As the Cl⁻ ligand can be easily hydrolysed in aqueous solutions, for both samples the metal species reacting with the protein in solution may be identical, and indeed the mass spectra of the two mixtures were very similar (Figure AI.5–6). The new band formation in the semi–native gel and the signal at M = 10458 Da indicated that both complexes lost their axial ligands and coordinated to the protein in the same way, possibly to the haem–binding pocket of the protein. For **Co3**, which is a Schiff base metal complex with a square planar geometry that has two axial positions available for ligand coordination, exceptionally fast protein–complex binding was found.[20,21] In solution, solvent molecules may typically coordinate the metal, and in the ArM preparation conditions it is hence likely that **Co3** bears one or two aqua molecules coordinated to the metal center. According to the SDS–gels and mass spectrometry analysis, these ligands are labile enough to allow fast binding of **Co3** to the protein, not only in the pocket but also to outer residues of the protein. Finally, **Co4** was the largest complex in our library, and it showed no interaction with **apoCB5.** It is a good negative control in the series, showing that steric interaction may avoid the insertion of an artificial cofactor into the protein pocket of a protein, and that not all cofactors based on cobalt can be put in this particular protein scaffold.

Last but not least, in theory the structure of the protein may also play a role in the formation of the ArM but for *apo*Myb similar results were found compared to *apo*CB5, for example the cobalt complexes **Co1** and **Co3**, even if the binding pocket of the two proteins are different (Chapter 1). Besides those located in the binding pocket, **Myb** has more than seven histidine residues in its sequence. The only difference observed between *apo*CB5 and *apo*Myb was with **Co4**, which showed a new band for *apo*Myb but not for *apo*CB5. However, the LC chromatogram of the mixture showed that the *apo*Myb–**Co4** adduct was more hydrophobic than *apo*CB5, suggesting that the complex may bind in the outer shell of the protein (Figure AI.12). For **Co1** the MS spectra (Figure AI.10) showed signals corresponding to the complex bound to *apo*Myb still bearing both axial Cl⁻ ligand, which was a striking difference with *apo*CB5–**Co1**. Overall, these results point to the difference in size of the haem–binding pocket of the two proteins, which may be larger for **Myb** and adapt better larger cobalt cofactors such as **Co4**.

2.4. Conclusion

A novel screening method based on SDS–page was developed to check the interaction between the *apo* forms of two haem proteins, **CB5** and **Myb**, and a library of 7 WOCs: three Ruthenium complexes **Ru1**–**Ru3** and four cobalt complexes **Co1**–**Co4**. Most artificial cofactors could substitute either one or two of their axial monodentate ligands by coordinating residues of the proteins, thereby producing an ArM. Semi–native SDS–gel was found to give the best resolution for studying by gel electrophoresis ArM formation. During ArM preparation, the catalyst concentration was found to be very important for maximizing the formation of the desired 1:1 adduct, while keeping the temperature low (4 °C) was required to prevent protein denaturation. On the other hand, the pH of the buffer had no significant effect on the binding of the catalyst to the *apo* protein. Overall, the optimum incubation time was found much shorter for cobalt than for ruthenium complexes, which fits the expected lability of first–row *vs*. second–row transition metal centres. However, the

interaction of the metal complex with the protein was also strongly dependent on the nature of the complex, i.e., on the nature of the axial ligand(s) and on the hydrophilicity, charge, size, and aromaticity of the planar tetradentate ligand bound to the metal complex. Five complexes from our library showed on SDS–page clear binding to *apo*CB5: **Ru2**, **Ru3**, **Co1**, **Co2** and **Co3**. This interaction was confirmed by ESI–MS, which allowed to characterize the protein–complex adduct. In fact, only the combined use of SDS page and mass spectrometry allows to conclude on the formation of an ArM. Finally, all haem proteins are not equivalent: for *apo*Myb, two complexes only (**Co1** and **Co3**) showed protein binding, the latter being able to bind several molecules of the complex to the protein.

2.5. Experimental section

2.5.1. Materials and methods

All chemicals were of analytical grade and were purchased from Sigma Aldrich unless otherwise specified. Complex N,N'–Bis(salicylidene)ethylenediaminocobalt (II) (catalyst **Co1**) was purchased from Alfa Aesar. Purified water was obtained using a Milli–Q system (Advantage A10). Myoglobin (**Myb**) from equine skeletal muscle was commercially obtained from Sigma Aldrich (M0630–1G, Missouri, USA). HR–MS was performed in a Thermo Scientific Q Exactive Orbitrap (ESI+) coupled to a Ultimate 3000 nanosystem (3.5 kV; 275 °C; Resolution R = 240.000 at m/z = 400; external lock; mass range m/z = 150–1500); Mobile phase MeCN/H_2O (1;1 v/v) with 0.1 % formic acid, flow = 25 µl/min direct injection of a 1 µM sample conc. ESI–MS was performed on a Synapt G2–Si mass spectrometer from Waters, initial separation and denaturing of protein samples was achieved using a C4 reversed phase column. Samples were prepared in 10 mM NH_4Ac buffer at pH 7.0 a using Micro Bio–Spin p6 gel desalting columns (Bio–Rad, # 7326221), maximally 30 min before being run. Deconvolution was performed using the MaxEnt. Algorithm of the MassLynx software. (Semi–native) Gel electrophoresis was performed using 15 % polyacrylamide gels containing 0.1 % sodium dodecyl

sulphate (SDS). Cracking buffer semi–native PAGE was prepared in absence of SDS and β–mercaptoethanol. The gels were run on a (Mini–Protean System and PowerPac Basic Power Supply from Bio–Rad, California, USA) for 50 min. at 200 V. The gels were imaged with 2,2,2–trichloroethanol (5 µL per mL was added to the gel mixture, Sigma–Aldrich)[22] or coomassie brilliant blue (gels were fixed prior to staining) as specified with each figure, using a Gel Doc XR+ from Bio–Rad (#170–8195). Gel images were processed using the Image lab Software version 6.01 from Bio–Rad, adjusting the gamma setting to improve the contrast.

2.5.2. Expression and purification of bovine cytochrome B5 (CB5)

The plasmid for expression of **CB5** was kindly provided by the Prof. Ubbink lab at Leiden Institute of Chemistry. CB5 was expressed in *Escherichia coli* BL21 PLysS, grown semi–anaerobically in 2L Erlenmeyer's containing 1.7 L Lysogeny broth (LB) with 0.1 mM kanamycin and 0.1 mM chloramphenicol at 37 °C. Growth was continued until an optical density (OD600) of 0.550 was reached, overexpression of haem was then induced using δ–aminolaevulinic acid hydrochloride. Growth was continued until an OD600 of 0.6–0.8 was reached, protein overexpression was then induced using 1 mM isopropyl β–D–1–thiogalactopyranoside (IPTG) and performed overnight. The light pink cell cultures were pelleted using a Sorval RC 6+ centrifuge from Thermo scientific (Massachusetts, USA) at 6000 rpm and 4 °C. Cell pellets were washed once with a 150 mM NaCl solution, then resuspended in 20 mM sodium phosphate (NaPi) buffer at pH 7.4 with 150 mM NaCl. Cells with added DNase, phenylmethylsulphonyl fluoride (PMFS) and lysozyme were broken up by sonification in an ice bath using a Branson Digital Sonifier (Emerson Electric Missouri, USA) set to 30 %, 4 s – on, 5 s – off, for 7 min. Cell debris was removed by centrifugation with an Eppendorf centrifuge (5804 R, Hamburg, Germany) at 11000 rpm, 30 min, 4 °C. The resulting solution was mixed with a 1 M KCl stock to a final concentration of 0.4 M and 6 % w/v PEG4000, then centrifuged again. The protein solution was dialysed overnight

against 2 L of 20 mM NaPi pH 7.4 with one buffer exchange after 2 h, cellulose dialysis tubing from Spectrum Chemical (California, USA, #132725) was used with a cut–off of 3.5 kDa. A 300 mL gradient in 20 mM sodium phosphate, pH 7.5 from 0 to 0.5 M NaCl was employed to purify the protein over a DEAE column (HiTrap DEAE FF 5 mL from Sigma Aldrich, Missouri, USA), then a Q column (HiTrap Q HP 5 mL from Sigma Aldrich, Missouri, USA). Red fractions containing ***holo*CB5** were collected, combined, and concentrated using 20 mL, 5.000 kDa cut–off concentrators (Corning, New York, USA). ***Holo*CB5** was finally purified over 120 mL Superdex 75 pg HiLoad 16/600 column equilibrated with 20 mM sodium phosphate, 150 mM NaCl, pH 7.0, re–concentrated and stored frozen (with liquid N$_2$) at –80 °C until use. Concentration of the ***holo*CB5** was calculated also by UV–Vis measuring the absorbance at 280 nm band and using the extinction coefficient ε = 11460 M^{-1}cm^{-1} and the absorbance at 413 nm band corresponding to Haem and using the extinction coefficient ε = 117000 M^{-1}cm^{-1}.

2.5.3. Teale's method to prepare *apo* protein from Cytochrome B5 and Myoglobin

Haem extraction from proteins was performed using Teale's method.[23] To this end the pH of the protein was lowered to pH 2.0, by dropwise addition of 0.5 M HCl under constant stirring on ice. An equal volume of cold 2–butanone was added and mixed, then pipetted off after the layers separated, and this procedure was repeated a second time. The aqueous layer was pipetted directly into a 3.5 kDa cut–off dialysis bag (cellulose dialysis tubing from Spectrum Chemical, California, USA, #132725) and dialyzed against 2 L of 20 mM sodium phosphate, pH 7.4 at 4 °C overnight. The dialysis buffer was exchanged once after 2 h of dialysis. UV–Vis was used to verify the protein was in the *apo* form where the band of Haem (413 nm) was absent. Concentration of the ***apo*CB5** was calculated also by UV–Vis measuring the absorbance at 280 nm band and using the extinction coefficient ε = 11460 M^{-1}cm^{-1}.

2.5.4. Synthesis

2.5.4.1. Synthesis of [2,2':6',2''–terpyridine]–6,6''–dicarboxylic acid (tpyda)
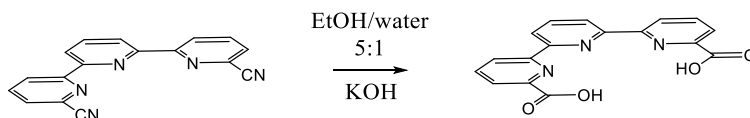
Compound was synthetized following the procedure described on literature.[24] In a 250 mL round–bottom flask were added 2,2':6',2''–terpyridine–6,6''–dicarbonitrile (1.5 g, 5.29 mmol), ethanol (100 mL) and water (20 mL). Then KOH pellets (2.8 g, 49.9 mmol) were added to the mixture. The reaction mixture was refluxed for overnight. TLC performed in Hexane/EtOAc (9:1) showed consumption of 6,6"–dicarbonitrile–2,2';6,2"–terpyridine . Then the solvent was removed with rotavap, the white residue was dissolved in water (100 mL), and the pH was adjusted to 4 with aqueous HCl (1 M) upon which a white precipitate appeared. The precipitate was removed by filtration and washed sequentially with cold water (100 mL) and acetonitrile (100 mL). Afterward, the solid was heated to reflux in a mixture of concentrated H_2SO_4 / concentrated CH_3COOH (100 mL, 1:1) for 5 h. The reaction mixture was then poured onto ice. A white solid precipitate which was filtered and washed with cold water (100 mL) and acetonitrile (100 mL). The white solid was dried overnight under vacuum. LCMS: [M+2H] = 322.4. ^1H–NMR (400 MHz, DMSO) δ 13.34 (s, 2H), 8.88 (dd, 2H), 8.66 (d, 2H), 8.22 (t, 3H), 8.16 (dd, 2H).Yield: 70%.

2.5.4.2. Synthesis of [Ru(II)((tpyda)(DMSO)(H$_2$O)] (Ru1)
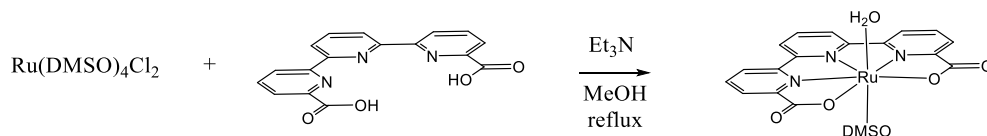
The compound was synthetized following the procedure described in the literature.[25] [Ru(DMSO)$_4$Cl$_2$] (300 mg, 0.308 mmol), 2,2':6',2''–terpyridine–6,6''–dicarboxylic acid (200 mg, 0.622 mmol), and triethylamine (0.6 mL, 4.30 mmol)

were dissolved and degassed in dry methanol (6 ml), refluxed for 6 h, and cooled down to room temperature. A brown solid (100 mg) appeared in the reaction mixture and that was filtered and washed with methanol (3 x 30 mL) and diethyl ether (3 x 30 mL). The solid was dissolved in water (30 mL), and the mixture was heated at 60 °C until all solids were dissolved. Then, the solvent was evaporated, and the resulting solid was washed with acetone (100 mL) and diethyl ether (100 mL) and dried under vacuum. ^{1}H–NMR (400 MHz, D$_2$O) δ 8.33 (dd, 2H), 8.31 (d, 2H), 8.16 (t, 2H), 8.06 (t, 1H), 8.01 (d, 2H). Yield: 57%.

2.5.4.3. Synthesis of 2,2':6',2'':6'',2'''–quaterpyridine (qpy)
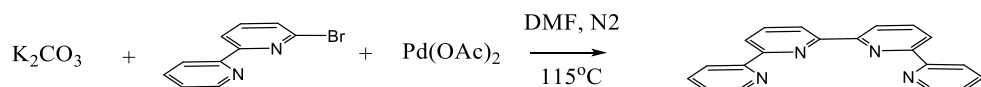
The compound was synthetized following the procedure described in the literature.[26] 6–bromo–2,2'–bipyridine (300 mg, 1.276 mmol), N–tetrabutylammonium bromide (206.3 mg, 0.640 mmol), diacetoxypalladium (43 mg, 0.192 mmol) and potassium carbonate (176 mg, 1.276 mmol) were placed in a 25 mL dry round–bottom flask and dissolved in dry DMF (2 mL). The solution was stirred under N$_2$ atmosphere for a few minutes (15–20 min) at 115 °C. Then Isopropanol (8 mL) was added to the orange solution and the mixture was stirred for 3h at 115 °C. After cooling to room temperature, water and ether (50 mL each) were added and the organic phase was extracted and dried over MgSO$_4$. The solvent was removed under vacuum to obtain a pale–yellow solid. The first ^{1}H–NMR in CDCl$_3$, showed signals of the starting material. After washing the product with Acetonitrile (15 mL) the pure compound was obtained according ^{1}H–NMR. ^{1}H–NMR (400 MHz, CDCl$_3$) δ 8.75 (dd, 2H), 8.70 (dd, 4H), 8.51 (dd, 2H), 8.03 (td, 2H), 7.91 (t, 2H), 7.38 (dd, 2H). Yield: 21.4%.

2.5.4.4. Synthesis of N,N'–(1,2–phenylene)dipicolinamide
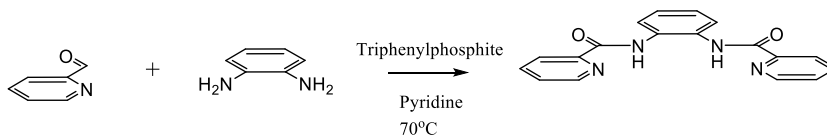
The compound was synthetized following the procedure described in literature.[27] Benzene–1,2–diamine (0.55 g, 5.09 mmol) and triphenyl phosphite (2.5 ml, 5.09 mmol) were added to a stirred solution of picolinic acid (1.252 g, 10.17 mmol) in pyridine (5 mL). The yellow solution was heated at 70 °C over night. Evaporation of the solvent gave a brown solid which was washed with H_2O/MeOH (1:1) (60 mL) and Et_2O (2 x 30 mL) to yield the product as an off–white solid. ^{1}H– NMR (400 MHz, $CDCl_3$) δ 10.26 (s, 2H), 8.56 (ddd, 2H), 8.32 (dt, 2H), 7.89 (m, 4H), 7.46 (ddd, 2H), 7.31 (dd, 2H). Yield: 45%.

2.5.4.5. Synthesis of [Ru(II)(N,N'–(1,2-phenylene)dipicolinamide) (CO) (H_2O)] (Ru2)
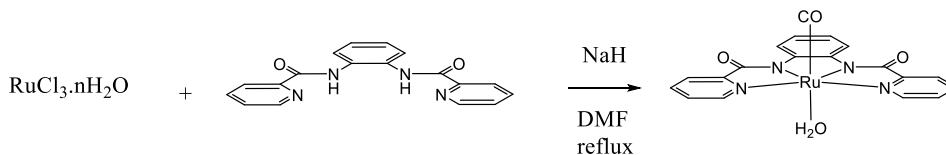
The compound was synthetized following the procedure described in the literature.[27] To a stirred solution N,N'–(1,2–phenylene)dipicolinamide (150 mg, 0.471 mmol) and sodium hydride (22.56 mg, 0.94 mmol) in dry DMF (4 mL) was added $RuCl_3 \cdot nH_2O$ (150 mg, 0.471 mmol). The reaction mixture was refluxed under nitrogen over night after which the solvent was evaporated under reduced pressure. MeCN (10 mL) was added to the residue and the black precipitate was filtered off. After the addition of H_2O (10 mL), the mixture was let to stand in the fridge over night to form a dark–green precipitate. Filtering and washing with H_2O (100 mL) gave the title complex as a dark–green solid. ^{1}H–NMR (400 MHz, MeOD) δ 9.03 (d,

2H), 8.64 (dd, 2H), 8.17 (t, 2H), 8.08 (d, 2H), 7.69 (td, 2H), 7.05 (dd, 2H)   Yield: 14% .

2.5.4.6. Synthesis of [Co(II)(qpy)(Cl)$_2$]·2H$_2$O (Co1)
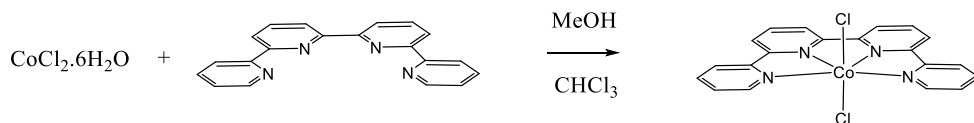
Compound was synthetized following the procedure described in the literature.[28]   CoCl$_2$.6H$_2$O (33.3 mg, 0.140 mmol) was dissolved in methanol (3 mL). A solution of 2,2':6',2'':6'',2'''–quaterpyridine (43.3 mg, 0.140 mmol) in chloroform (2 mL) was added slowly with stirring. A brown solid was formed gradually and the mixture was stirred for 2 h under air. The solid was filtered and washed with methanol and chloroform to remove the unreacted ligand. The solid was dried in air. Yield: 57%.

2.5.4.7. Synthesis of [Co(II)(qpy)(H$_2$O)$_2$](ClO$_4$)$_2$ (Co2)
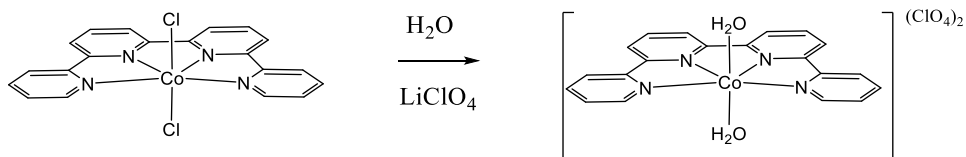
The compound was synthetized following the procedure described in the literature.[28] **Co1** (21.23 mg, 0.048 mmol) was dissolved in water (2.5 mL). Lithium perchlorate (14.64 mg, 0.138 mmol) was added to the solution with stirring under air. A pale brown solid precipitated gradually and the solution was stirred for 30 min. The solid was collected by filtration, washed with water and diethyl ether and dried in air. Yield: 31%.

2.5.4.8. Synthesis of [Ru(II)(qpy)(Cl)$_2$] (Ru3)
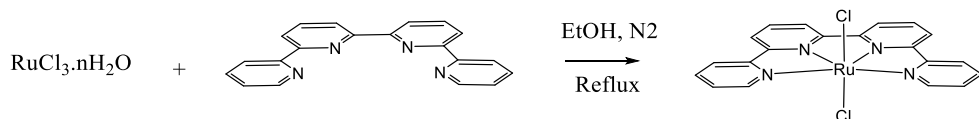
The compound was synthetized following the procedure described in the literature.[29]   A solution of 2,2':6',2'':6'',2'''–quaterpyridine (49.5 mg, 0.159 mmol) and RuCl$_3$.3H$_2$O (39 mg, 0.159 mmol) in 5 mL of dry and degassed ethanol were refluxed under argon for 12 h. After cooling to room temperature a green solid precipitated was filtered, washed with water (2 x 30 mL) and diethyl ether (2 x 50 mL). *LCMS* m/z calc: 487.9 , found:[M–Cl+CH$_3$CN] = 488.1. Yield: 91%.

2.5.5. Incubation with metal complexes for gel screening

Stock solution of each complex was prepared prior incubation. In experiments including the full library of Ru– and Co–complexes, complexes **Co1**, **Co3** and **Ru1** were dissolved in distilled water, while **Co4**, **Ru2**, and **Ru3** were dissolved in dimethyl sulfoxide (DMSO) and **Co2** in a mixture of 60:40 DMSO/distilled water, giving a final concentration of 10 % DMSO in the samples used in these experiments. *Apo* proteins were reacted with one of the transition–metal catalysts by mixing 10 μM of the *apo* protein in 20 mM sodium phosphate buffer at pH 6.5, 7.0, 7.5 or 8.0 with 10 μM, 50 μM or 100 μM catalyst (protein: catalyst molar ratio 1:1, 1:5 or 1:10) by adding 5 μL of 1 mM catalyst to 45 μL of protein solution. All reactions were performed over 24 – 48 h at 4 °C under constant agitation in the dark.

2.6. References

(1)   Opdam, L. V.; Polanco, E. A.; de Regt, B.; Lambertina, N.; Bakker, C.; Bonnet, S.; Pandit, A. A Screening Method for Binding Synthetic Metallo–Complexes to Haem Proteins. *Analytical Biochemistry* **2022**, *653*, 114788. https://doi.org/10.1016/j.ab.2022.114788.

(2)   Natoli, S. N.; Hartwig, J. F. Noble−Metal Substitution in Hemoproteins: An Emerging Strategy for Abiological Catalysis. *Acc. Chem. Res.* **2019**, *52* (2), 326–335. https://doi.org/10.1021/acs.accounts.8b00586.

(3)   Kerns, S. A.; Biswas, A.; Minnetian, N. M.; Borovik, A. S. Artificial Metalloproteins: At the Interface between Biology and Chemistry. *JACS Au* **2022**, *2* (6), 1252–1265. https://doi.org/10.1021/jacsau.2c00102.

(4)   Tian, L.; Li, Z.; Xu, X.; Zhang, C. Advances in Noble Metal (Ru, Rh, and Ir) Doping for Boosting Water Splitting Electrocatalysis. *J. Mater. Chem. A* **2021**, *9* (23), 13459–13470. https://doi.org/10.1039/D1TA01108A.

(5)   Ye, S.; Ding, C.; Liu, M.; Wang, A.; Huang, Q.; Li, C. Water Oxidation Catalysts for Artificial Photosynthesis. *Adv. Mater.* **2019**, *31* (50), 1902069. https://doi.org/10.1002/adma.201902069.

(6)   Nesterov, D.; Nesterova, O. Polynuclear Cobalt Complexes as Catalysts for Light–Driven Water Oxidation: A Review of Recent Advances. *Catalysts* **2018**, *8* (12), 602. https://doi.org/10.3390/catal8120602.

(7)   Chen, Q.–F.; Guo, Y.–H.; Yu, Y.–H.; Zhang, M.–T. Bioinspired Molecular Clusters for Water Oxidation. *Coordination Chemistry Reviews* **2021**, *448*, 214164. https://doi.org/10.1016/j.ccr.2021.214164.

(8)   Garfin, D. E. Chapter 29 One–Dimensional Gel Electrophoresis. In *Methods in Enzymology*; Elsevier, 2009; Vol. 463, pp 497–513. https://doi.org/10.1016/S0076–6879(09)63029–9.

(9)   Hirano, H.; Shirakawa, J. Recent Developments in Phos–Tag Electrophoresis for the Analysis of Phosphoproteins in Proteomics. *Expert Review of*

Proteomics **2022**, *19* (2), 103–114. https://doi.org/10.1080/14789450.2022.2052850.

(10) Huang, D. Y.; Khan, K. Characterization and Quantification of Native Glutenin Aggregates by Multistacking Sodium Dodecyl Sulfate Polyacrylamide Gel Electrophoresis (SDS–PAGE) Procedures. *Cereal Chemistry Journal* **1997**, *74* (3), 229–234. https://doi.org/10.1094/CCHEM.1997.74.3.229.

(11) Schägger, H. Tricine–SDS–PAGE. *Nat Protoc* **2006**, *1* (1), 16–22. https://doi.org/10.1038/nprot.2006.4.

(12) Nowakowski, A. B.; Wobig, W. J.; Petering, D. H. Native SDS–PAGE: High Resolution Electrophoretic Separation of Proteins with Retention of Native Properties Including Bound Metal Ions. *Metallomics* **2014**, *6* (5), 1068–1078. https://doi.org/10.1039/C4MT00033A.

(13) Kozlowski, L. P. IPC 2.0: Prediction of Isoelectric Point and pKa Dissociation Constants. *Nucleic Acids Research* **2021**, *49* (W1), W285–W292. https://doi.org/10.1093/nar/gkab295.

(14) Meersman, F.; Smeller, L.; Heremans, K. Protein Stability and Dynamics in the Pressure–Temperature Plane. *Biochimica et Biophysica Acta (BBA) – Proteins and Proteomics* **2006**, *1764* (3), 346–354. https://doi.org/10.1016/j.bbapap.2005.11.019.

(15) Jaenicke, R.; Böhm, G. The Stability of Proteins in Extreme Environments. *Current Opinion in Structural Biology* **1998**, *8* (6), 738–748. https://doi.org/10.1016/S0959–440X(98)80094–8.

(16) Moriyama, Y.; Kondo, N.; Takeda, K. Secondary Structural Changes of Homologous Proteins, Lysozyme and α–Lactalbumin, in Thermal Denaturation up to 130 °C and Sodium Dodecyl Sulfate (SDS) Effects on These Changes: Comparison of Thermal Stabilities of SDS–Induced Helical Structures in These Proteins. *Langmuir* **2012**, *28* (47), 16268–16273. https://doi.org/10.1021/la3035598.

(17) Kojima, T.; Sakamoto, T.; Matsuda, Y. Toward a Photochemical and Thermal Molecular Machine: Reversible Ligand Dissociation and Binding in a Ruthenium(II)–2,2'–Bipyridine Complex with Tris(2–Pyridylmethyl)Amine. *Inorg. Chem.* **2004**, *43* (7), 2243–2245. https://doi.org/10.1021/ic035137f.

(18) van Rixel, V. H. S.; Siewert, B.; Hopkins, S. L.; Askes, S. H. C.; Busemann, A.; Siegler, M. A.; Bonnet, S. Green Light–Induced Apoptosis in Cancer Cells by a Tetrapyridyl Ruthenium Prodrug Offering Two Trans Coordination Sites. *Chem. Sci.* **2016**, *7* (8), 4922–4929. https://doi.org/10.1039/C6SC00167J.

(19) Matsuo, H.; Toganoh, M.; Ishida, M.; Mori, S.; Furuta, H. Stereoretentive Ligand Exchange Reactions of N–Fused Porphyrin Ruthenium(II) Complexes. *Inorg. Chem.* **2017**, *56* (22), 13842–13851. https://doi.org/10.1021/acs.inorgchem.7b01972.

(20) Pui, A.; Policar, C.; Mahy, J.–P. Electronic and Steric Effects in Cobalt Schiff Bases Complexes: Synthesis, Characterization and Catalytic Activity of Some Cobalt(II) Tetra–Halogens–Dimethyl Salen Complexes. *Inorganica Chimica Acta* **2007**, *360* (6), 2139–2144. https://doi.org/10.1016/j.ica.2006.10.040.

(21) Park, S.; Mathur, V. K.; Planalp, R. P. Syntheses, Solubilities and Oxygen Absorption Properties of New Cobalt(Ll) Schiff–Base Complexes. 6.

(22) Ladner, C. L.; Yang, J.; Turner, R. J.; Edwards, R. A. Visible Fluorescent Detection of Proteins in Polyacrylamide Gels without Staining. *Analytical Biochemistry* **2004**, *326* (1), 13–20. https://doi.org/10.1016/j.ab.2003.10.047.

(23) Teale, F. W. J. Cleavage of the Haem–Protein Link by Acid Methylethylketone. *Biochimica et Biophysica Acta* **1959**, *35*, 543. https://doi.org/10.1016/0006–3002(59)90407–X.

(24) Galaup, C.; Couchet, J.–M.; Bedel, S.; Tisnès, P.; Picard, C. Direct Access to Terpyridine–Containing Polyazamacrocycles as Photosensitizing Ligands for

Eu(III) Luminescence in Aqueous Media. *J. Org. Chem.* **2005**, *70* (6), 2274–2284. https://doi.org/10.1021/jo0480242.

(25)   Matheu, R.; Benet–Buchholz, J.; Sala, X.; Llobet, A. Synthesis, Structure, and Redox Properties of a *Trans* –Diaqua Ru Complex That Reaches Seven–Coordination at High Oxidation States. *Inorg. Chem.* **2018**, *57* (4), 1757–1765. https://doi.org/10.1021/acs.inorgchem.7b02375.

(26)   Wachter, E.; Zamora, A.; Heidary, D. K.; Ruiz, J.; Glazer, E. C. Geometry Matters: Inverse Cytotoxic Relationship for Cis/Trans–Ru(II) Polypyridyl Complexes from Cis/Trans–[PtCl $_2$ (NH $_3$) $_2$]. *Chem. Commun.* **2016**, *52* (66), 10121–10124. https://doi.org/10.1039/C6CC04813G.

(27)   Kärkäs, M. D.; Åkermark, T.; Chen, H.; Sun, J.; Åkermark, B. A Tailor–Made Molecular Ruthenium Catalyst for the Oxidation of Water and Its Deactivation through Poisoning by Carbon Monoxide. *Angewandte Chemie International Edition* **2013**, *52* (15), 4189–4193. https://doi.org/10.1002/anie.201210226.

(28)   Leung, C.–F.; Ng, S.–M.; Ko, C.–C.; Man, W.–L.; Wu, J.; Chen, L.; Lau, T.–C. A Cobalt(Ii) Quaterpyridine Complex as a Visible Light–Driven Catalyst for Both Water Oxidation and Reduction. *Energy Environ. Sci.* **2012**, *5* (7), 7903. https://doi.org/10.1039/c2ee21840b.

(29)   Liu, Y.; Ng, S.–M.; Yiu, S.–M.; Lam, W. W. Y.; Wei, X.–G.; Lau, K.–C.; Lau, T.–C. Catalytic Water Oxidation by Ruthenium(II) Quaterpyridine (Qpy) Complexes: Evidence for Ruthenium(III) Qpy– *N* , *N'''* –Dioxide as the Real Catalysts. *Angew. Chem.* **2014**, *126* (52), 14696–14699. https://doi.org/10.1002/ange.201408795.